

Development of spatial turbulence from boundary-controlled patterns in class-B lasers

Eduardo Cabrera,* Oscar G. Calderón,† Sonia Melle, and J. M. Guerra

Departamento de Óptica, Universidad Complutense de Madrid, Ciudad Universitaria s/n, 28040 Madrid, Spain

(Received 1 February 2006; published 23 May 2006)

We report time-resolved measurements of transverse dynamics in a pulsed custom-made Nd:YAG (yttrium aluminum garnet) broad-area laser, where a dynamic transition from order to turbulentlike patterns appears, without the modification of the Fresnel number. To our knowledge, it is the first time this dynamical transition is observed in a class-B laser. Higher values of the pumping and a higher ratio between the electric field and the inversion population decay rates diminish the time at which the transition takes place. A theoretical model based on the adiabatic approximation allows us to explain the main features of the observed dynamics and to compare the results with those previously seen, especially in broad-area CO₂ lasers.

DOI: [10.1103/PhysRevA.73.053820](https://doi.org/10.1103/PhysRevA.73.053820)

PACS number(s): 42.65.Sf, 42.60.Jf, 42.60.Mi

I. INTRODUCTION

Class-B lasers are defined as those in which the polarization decay rate is greater than the electric field decay rate and at the same time this one is also larger than the population decay rate. They have received a great amount of attention in the study of pattern formation in broad-area lasers. Single vortex [1], vortex lattices [2], high order structures, and turbulence [3,4], are only a few examples of the large variety of spatio-temporal dynamics that have been observed in these lasers. Besides the importance from the fundamental point of view, class-B lasers play a crucial role in industrial applications [5], in medicine [6], or in communications [7] to cite just a few. Therefore, the study of the spatial profile of the laser field becomes a relevant problem since it allows us to determine the spatial coherence and the brilliance of the laser beam.

A great variety of stationary spatial structures have been observed in vertical cavity surface emitting lasers (VCSELs) for different configurations of the resonator. Hegarty *et al.* observed for the first time the standing wave (stripelike pattern) predicted by the Maxwell-Bloch equations [8]. Ackemann *et al.* [9] and Babushkin *et al.* [10] showed different symmetry properties of the stationary patterns for lasers with very close operating conditions, due to a competition process between rotational symmetry imposed by the circular aperture and Cartesian symmetry imposed by anisotropies. They observed rotational symmetry patterns such as “flowerlike” patterns, and Cartesian symmetry patterns such as Hermite-Gaussian modes and tilted waves. Stable square vortex lattices have been obtained in solid-state microchip lasers by Chen and Lan [2,11]. This kind of pattern has also been found in CO₂ lasers [12,13]. Experimental works in CO₂ lasers by Huyet *et al.* showed a chaotic local intensity, leading to the loss of spatial correlation in the transverse section of the laser, although high-order time-averaged patterns were measured [14,15]. This seems to indicate that the pattern develops a fast and irregular dynamics. Instantaneous measurements of patterns have been done in regular semiconduc-

tor lasers with only one relevant transverse dimension. This allows to measure the time evolution of the one-dimensional (1D) instantaneous pattern by using a single-shot streak camera with a time resolution of approximately 50 ps [16]. They observed the formation and migration of filamentary structures along the pattern. This result shows that very disordered dynamics can be masked by average measurements.

Two-dimensional instantaneous patterns were measured for the first time by Encinas-Sanz *et al.* in a pulsed CO₂ laser [3,4]. Static filamentary structures (optical filaments) are created and annihilated in the transverse section of the laser continuously during the whole evolution of the pulse with a lifetime of 2 ns. However, in spite of this turbulent behavior, the average pattern shows eight or nine rolls whose orientation is determined by boundary conditions.

Other studies of pattern formation in class-B lasers have been done in Nd:YAG (yttrium aluminum garnet) lasers. Hollinger *et al.* studied transverse mode dynamics in a ring resonator [17]. They found a transition from stable to periodic, quasiperiodic and chaotic temporal behavior of the laser by increasing the Fresnel number of the cavity $F=(b/2)^2/\lambda L$, where b is the transverse size, L is the cavity length, and λ is the wavelength of the laser field. This parameter measures the aspect ratio between the aperture area and the length of the cavity and roughly gives an estimation of the number of modes that can oscillate in the laser [18]. Q -switched Nd:YAG lasers have also been studied for stable and unstable resonator configurations [19]. In that case, instantaneous transverse patterns were recorded showing that a Gaussian profile of the beam was selected by the system in the stable configuration along the whole evolution of the pulse, while the unstable resonator caused the growing of a ring shaped profile. However, it must be pointed out that no disordered patterns or high-order modes were found in these configurations.

In this paper, we report time-resolved measurements of transverse dynamics in a pulsed custom-made Nd:YAG broad-area laser, where a transition from order to turbulentlike patterns dynamically appears, without the modification of the Fresnel number. It can be seen how the pattern initially grows under the influence of boundary conditions, so mode-like patterns appear. After that, nonlinearities of the medium govern the evolution and the ordered structures are unstabi-

*Electronic address: ecabrera@fis.ucm.es

†URL: <http://www.ucm.es/info/laserlab>

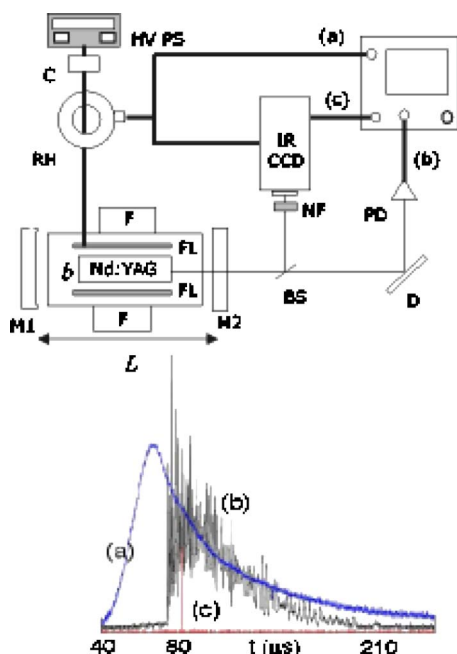


FIG. 1. (Color online) (Top) Experimental setup to measure the instantaneous intensity pattern of our broad-area Nd:YAG laser. FL, flash-lamps; F, fans for air cooled system; HV PS, high voltage power supply; C, capacitor $100 \mu\text{F}$; RH, Rodowsky Hall; M1, concave (10 m radius); total reflector; M2, plane output couple (70% reflectivity); BS, beam splitter, NF, filter to avoid overexposure of the camera; IR CCD, camera; D, diffusor; PD, photodiode; O, oscilloscope. (Bottom) Signals recorded in the transient programmable digitizer: (a) pump time profile, (b) output intensity, (c) internal shutter of the camera.

lized towards a highly disordered pattern, which cannot be described by cavity modes. This dynamical transition has not been seen in any other type of class-B lasers. The highly disordered spatial dynamics observed in CO_2 lasers appears in all the registered times. No ordered phase in its evolution has been seen up to now, even though the Fresnel number of the resonator was five times smaller than the Fresnel number of the Nd:YAG laser resonator used in this work. This result shows that, apparently, the classification of lasers according to the ratio between decay rates is not enough to classify their spatial dynamics, and more parameters are needed to describe not only the quantitative features but the qualitative ones. In this paper we will try to tackle the problem to see what is the physical reason for this different behavior.

II. EXPERIMENTAL SETUP

The experimental setup is shown in Fig. 1. The single-shot laser is an air cooled, low pulse energy ($\approx 50 \text{ mJ}$) flash-lamp pumped prototype fired by means of an electronic switch. The lasing medium was a Nd:YAG cylindrical rod (60 mm long \times 6 mm diameter), side pumped by two parallel linear flash lamps. The rod and the flash-lamps are located inside a double elliptical gold-plated cylindrical pumping cavity. Inside this cavity, the two linear flash lamps are placed at the focus of the ellipses along the cylindrical cavity

while the rod is placed between them in the same horizontal plane. In this form, the pumping geometry imposes an anisotropy that selects a “Cartesian symmetry” instead of a circular symmetry. The lamps were excited by a $100 \mu\text{F}$ capacitor allowing a maximum of 1600 V to be applied to the lamps. The $L=17 \text{ cm}$ long laser resonator consists of a concave ($R=10 \text{ m}$ radius) total reflector and a plane output coupler (70% reflectivity). A nonpolarizing beam splitter (50:50) was placed behind the output coupler to separate the beam. The transmitted beam is carried to a photodiode (1 ns rise time) after reflecting on a magnesium diffusor to ensure we are measuring a spatially averaged intensity. The signal from the photodiode was measured in a transient programmable digitizer having a 1 GHz real time bandwidth. The reflected beam from the beam splitter reaches an intensified IR enhanced charge-coupled device (CCD) camera (4 Quick E, Stanford Computer Optics, Inc.), with a 768×494 pixels array. The spatial resolution is $50 \mu\text{m}/\text{pixel}$ which allows us to observe the spatial structure forming the pattern. The minimum integration time for the recorded patterns is 1 ns. This time must be compared with the characteristic time scale of the local intensity evolution. The measurement of the local intensity shows a time evolution of a few μs , which is the characteristic time of relaxation oscillations. It is well known that the frequency of the relaxation oscillations in cw class B lasers is $f_R^2 \approx 2\gamma_{\parallel}\kappa(R-1)/(2\pi)^2$ where $1/\kappa \approx 7 \text{ ns}$ is the photon lifetime, $1/\gamma_{\parallel} \approx 0.23 \text{ ms}$ is the population inversion lifetime, and R represents the dimensionless pumping parameter. For the range of pumping values used in our experiments (between 2.7 and 5), we obtain a frequency equal to $f_R \approx 0.3 \text{ MHz}$, which agrees with the experimental one. In conclusion, the instantaneous character of the recorded patterns is guaranteed. The laser operates in a single-shot regime leaving enough time between two shots to avoid thermal effects. We take one snapshot per pulse. Both the integration time and the time within the pulse at which we record the snapshots (time delay) are computer controlled. We use the electric signal that fires the flash-lamps as an external trigger to open the camera gate. A signal from the internal shutter of the camera is recorded in the transient programmable digitizer, where the output intensity and pump time profile are also recorded (see Fig. 1). Neutral filters in front of the camera aperture protects the system from overexposure.

III. EXPERIMENTAL RESULTS

In this section we study the evolution of the pattern along the pulse for a pump value 2.7 times above the threshold one. This pump is the lowest we can achieve with our setup. At the beginning of the output pulse we observe high-ordered structures although different kinds of modes appear. In particular, latticelike modes and stripelike modes are obtained, as can be seen in Fig. 2, which shows different kinds of ordered patterns recorded at the beginning of the laser pulse. An example of a lattice pattern which resembles a Gaussian-Hermite TEM_{45} is shown in Fig. 2(a). Stripelike modes with different orientations have also been observed [see Fig. 2(b), tilted 45° , and Fig. 2(c), vertical orientation]. The vertical

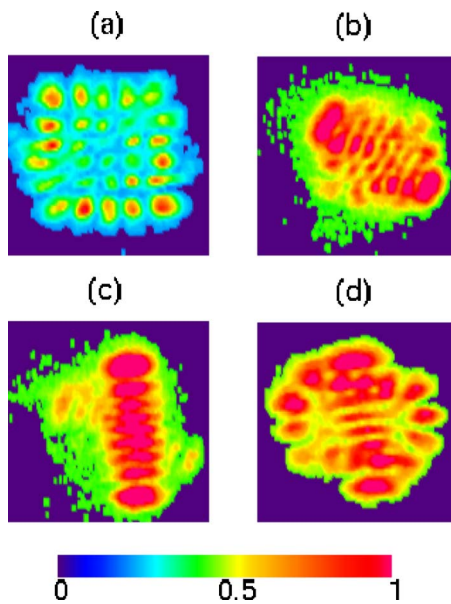


FIG. 2. (Color online) Experimental instantaneous intensity patterns (resolution time 9 ns) for a pumping 2.7 times above threshold. (a) and (b) for $4 \mu\text{s}$ of time delay from the beginning of the pulse, (c) for $8 \mu\text{s}$ of delay, and (d) for $40 \mu\text{s}$ of delay. Pattern size $6 \times 6 \text{ mm}$.

and horizontal directions correspond to the selected axis by the pump. This kind of pattern could be a standing wave or a high-order Gaussian-Hermite mode. In order to discern between both possibilities, the instantaneous far field patterns should be simultaneously measured with the near field ones. Figure 2(d) shows a more complex spatial profile that consists of a combination of a flowerlike pattern (characterized by bright peaks around the perimeter of the laser spot) with a stripelike pattern in the vertical direction. The characteristic length scale of all of these ordered structures is near 0.8 mm. The presence of this great variety of profiles for the same experimental conditions seems to indicate a weak selection of the spatial symmetry. As we mentioned in the Introduction, Babushkin *et al.* [10] and Ackemann *et al.* [9] showed a similar coexistence of patterns for VCSELs, for the case of stationary patterns. In that case, standing waves and structures close to high-order Gaussian-Laguerre modes were seen for the same experimental conditions. Only small anisotropies selected the pattern.

As time increases, bulk parameters dominate the dynamics, and the previous ordered structures disappear, leading to very disordered intensity profiles. Examples of this behavior can be seen in Fig. 3, which shows two instantaneous patterns recorded for a time delay of $80 \mu\text{s}$ approximately from the beginning of the output pulse. The pattern shown in Fig. 3(a) consists of a bunch of bright peaks randomly distributed over the transverse cross section, while superimposed traveling waves with different orientations can be seen in Fig. 3(b). In both of them, the mean size of the structures (around 0.2 mm) is much smaller than those present in the first steps of the emission. It must be pointed out that this characteristic length scale roughly remains constant during the rest of the evolution of the output pulse. Once the transition from order

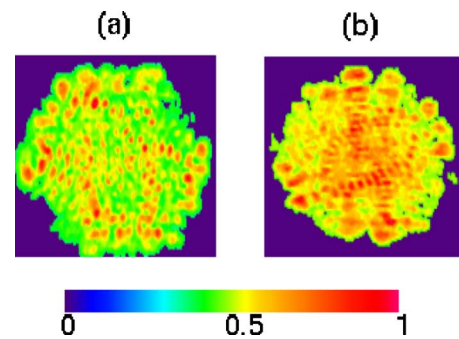


FIG. 3. (Color online) Experimental instantaneous intensity patterns (resolution time 9 ns) for a pumping 2.7 times above threshold. (a) for $77 \mu\text{s}$ of time delay from the beginning of the pulse and (b) for $83 \mu\text{s}$ of delay. Pattern size $6 \times 6 \text{ mm}$.

to disorder is complete, the pattern changes randomly but the mean size of the structures stays approximately unchanged.

Increasing the voltage applied to the flash lamps allows higher-order modes to overcome diffraction losses and thus, to appear. This can be seen in Figs. 4 and 5, which show characteristic intensity profiles recorded for a pump parameter 4 times above threshold and different times delays from the beginning of the emission. Figures 4(a)–4(c) show different profiles recorded in the ordered regime. It can be seen how the typical size of the structures reduces from those corresponding to lower pumping due to the mentioned appearance of higher-order modes. We have seen some high-order patterns [see Figs. 4(a) and 4(b)] which are very similar to those found by Chen *et al.* in Ref. [20]. They observed stationary transverse modes in a VCSEL which cannot be described by TEM modes or by the eigenfunctions of the Helmholtz equation with square rigid boundary conditions

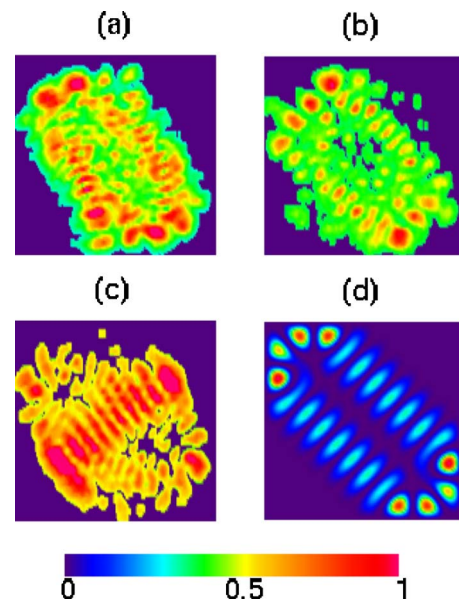


FIG. 4. (Color online) Experimental instantaneous intensity patterns (resolution time 3 ns) for a pumping 4 times above threshold. (a), (b), and (c) for $8 \mu\text{s}$ of time delay from the beginning of the pulse. Pattern size $6 \times 6 \text{ mm}$. (d) Transverse pattern calculated by using Eq. (3) in Ref. [20], $|\psi_{11}(x,y;3\pi/4) + \psi_{11}^*(x,y;3\pi/4)|^2$.

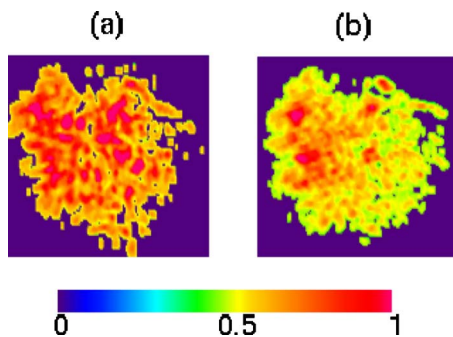


FIG. 5. (Color online) Experimental instantaneous intensity patterns (resolution time 3 ns) for a pumping 4 times above threshold. (a) for 23 μs of time delay from the beginning of the pulse and (b) for 25 μs . Pattern size 6 \times 6 mm.

[20]. In order to theoretically reproduce the measured patterns, they use SU(2) transverse mode functions which are based on the geometrical trajectories (see the detailed explanation in Ref. [21]). This kind of transverse modes are obtained through lateral boundary conditions. Using the same formalism, we have theoretically reproduced the patterns shown in Figs. 4(a) and 4(b) [see Fig. 4(d)]. Therefore, we could say that in this case the pattern formation is mainly governed by lateral boundary conditions. At larger times along the pulse, irregular intensity profiles appear as can be seen in Figs. 5(a) and 5(b). The characteristic size of the structures is much smaller than the one observed in the corresponding ordered patterns, i.e., we observe qualitatively the same behavior as described previously for lower voltages.

It is well known that the transversal size of high-order Gaussian-Hermite modes is approximately given by the expression $x_n \approx \sqrt{(n)}\omega(z)$ where n represents the mode order and $\omega(z)$ the size of the mode of zero order [22]. This approximation allows us to compare the sizes of the different modes that appear for different pumping values at the beginning of the output pulse. It can be demonstrated that the ratio between the transversal size of these modes is roughly the square root of the corresponding orders. This test supports the hypothesis of the appearance of Gaussian-Hermite modes in the beginning of the evolution of the laser field emission.

Higher pumping also causes changes in the dynamical transition from order to turbulence. In particular, we observe that the time when the transition takes place decreases as the pumping increases. However, we cannot give a precise relationship between this time and the pump value, due to the nonexact reproducibility of the pulsed laser. For the highest pump we can achieve, i.e., 5.4 times above threshold, no ordered patterns were observed in the times we measured.

IV. THEORETICAL DISCUSSION

A Nd:YAG laser is a case of an extreme class-B laser, due to the ratio between the time decay constants for electric field, electric polarization, and inversion of population. These are, respectively, $\kappa = 1.4 \times 10^8 \text{ s}^{-1}$, $\gamma_{\perp} = 4 \times 10^{11} \text{ s}^{-1}$, and $\gamma_{\parallel} = 4.35 \times 10^3 \text{ s}^{-1}$. Thus, we can handle the semiclassical

two-level Maxwell-Bloch equations in the adiabatic approximation. The use of a two-level model for a Nd:YAG laser is justified by the isomorphism between the complete four-level model for the Nd:YAG system and the standard two-level model, as was pointed out in Ref. [23]. Proper pumping and losses profiles complete the model. Therefore, the laser equations are the following:

$$\frac{\partial E}{\partial \tau} = ia\Delta_{\perp}E + \left(\frac{D}{1+i\delta} - \eta \right) E, \quad (1)$$

$$\frac{\partial D}{\partial \tau} = -\gamma \left[D - R + \frac{|E|^2 D}{1+\delta^2} \right]. \quad (2)$$

E and D are the dimensionless slowly varying envelopes of the electric field, and the population inversion, respectively. $\gamma \equiv \gamma_{\parallel}/\kappa$, $\delta = (\omega_{21} - \omega_c)/\gamma_{\perp}$ is the usual rescaled detuning between the atomic line center and the cavity frequency. Light diffraction is taken into account by means of the transverse Laplacian term in the field equation, and is measured by the diffraction coefficient $a = c^2/(2\omega_{21}\kappa b^2)$, where b is the spatial transverse size of the laser. $\Delta_{\perp} = \partial_x^2 + \partial_y^2$ is the transverse Laplacian where x and y are normalized with the spatial scale b . $\eta(x, y)$ takes into account the spatial dependence of the losses. This losses profile has been considered flat near the optical axis increasing strongly outside this area to account for diffraction. The time τ is normalized versus the electric field decay rate ($\tau = \kappa t$). $R(\tau, x, y)$ represents the pumping parameter. In order to reproduce the experimental conditions, we use a square spatial pumping profile. Likewise, the temporal form of the pumping was simulated by the following function approaching the pulse excitation of the lamps, which can be seen in Fig. 1,

$$R = A \left(\frac{\tau}{\tau_{peak}} \right)^3 e^{3(1-\tau/\tau_{peak})} \quad \text{for } \tau < \frac{5}{3}\tau_{peak},$$

$$R = A \left(\frac{5}{3} \right)^5 e^{-2\left(\frac{\tau_{peak}}{\tau} \right)^2} \quad \text{for } \tau \geq \frac{5}{3}\tau_{peak}, \quad (3)$$

where $\tau_{peak}/\kappa = 30 \mu\text{s}$ is the time needed for the pump to reach its maximum value. A has been chosen in order to obtain a total excitation energy above the threshold one corresponding to the potential charges used in the experiment.

The detuning value is not selected by any element inside the cavity. Thus, the system will choose the cavity mode with highest gain. We could roughly estimate this value measuring the characteristic size of the structures that appear in the beginning of the output pulse and considering the general result of the stability analysis for the case of a laser with infinite transverse section. Accordingly, the laser emission is off axis, with a transverse wave number $k_c = \sqrt{\delta/a}$. Taking into account both results, a detuning value as small as $\delta \approx 0.01$ is obtained. That so small a value will allow us to simplify the numerical calculations just taking a zero detuning. It must be pointed out that although we have used a result of the stability analysis for a laser with infinite transverse section, which of course it is not in our case, and in spite of the appearance of Gaussian-Hermite modes in the

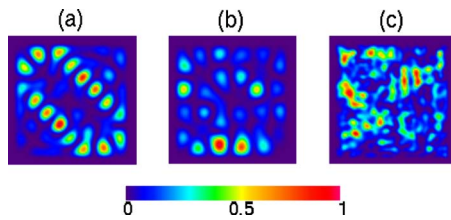


FIG. 6. (Color online) Simulated intensity patterns corresponding to different times along the laser pulse: at the beginning of the pulse (a) for $3 \mu\text{s}$, (b) for $5 \mu\text{s}$, and in the middle of the pulse (c) for $50 \mu\text{s}$. Those patterns were obtained for a pumping value of (a) 2 times above threshold, and (b),(c) 5 times above threshold.

first steps of laser emission, the estimation of the detuning value is still valid. The pattern first selected by the system must be that one with the highest gain-losses ratio, taking into account the restrictions imposed by boundary conditions. Although these restrictions can modify the size of the structures from those predicted by the stability analysis, a large discrepancy is not expected due to the high Fresnel number of the laser cavity. In any case, simulations have also been developed for different detuning values close to the previous one, showing no significant changes on the spatio-temporal dynamics. Thus, only the results with zero detuning will be presented.

Integration of the system of Eqs. (1) and (2) gives qualitative agreement with experimental results. In the first steps of the output emission, the calculated patterns show highly ordered structures, whereas turbulentlike patterns emerge for later times. This evolution can be seen in Fig. 6 which shows three representative instantaneous simulated patterns for different times along the pulse. The large variety of spatial distributions seen in the experiments have not been obtained. Flowerlike modes and latticelike modes appear in the ordered phase of the emission [see Figs. 6(a) and 6(b), respectively] but stripelike modes and more complex spatial distributions found in experiments have not been obtained. This could be explained by the strong influence of the boundary conditions used in our simulations which do not allow the appearance of this kind of modes.

Apart from these, other features of the dynamical evolution are reproduced by simulations. The reduction of the size of the structures along the pulse [which can be seen in Fig. 6(c)] and the decrease of the lifetime of a boundary-controlled regime for higher pumping have been corroborated with the simulations. These results show the validity of the model used, even with the simplicity of this model.

V. RELEVANCE OF THE RESULTS IN THE CONTEXT OF CLASS-B LASERS

Finally, let us discuss the relevance of our results in comparison with previous works related with patterns in class-B lasers. Although the studies of pattern formation in VCSELs provides a great variety of phenomena due to the possibility of obtaining huge Fresnel numbers, the extremely fast time evolution of the local intensity in semiconductor lasers makes it a very difficult task to record instantaneous snap-

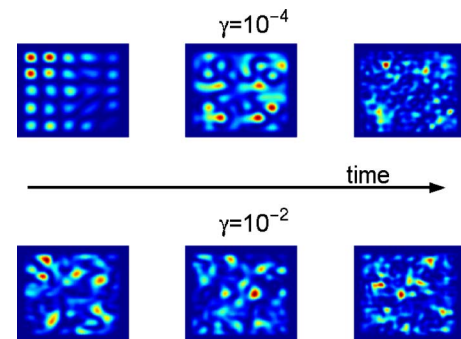


FIG. 7. (Color online) Simulated instantaneous patterns showing the evolution of the spatial intensity profile along the pulse for different values of $\gamma = \gamma_{||} / \kappa$. (Top) $\gamma = 10^{-4}$ (closer to the case of Nd:YAG lasers). (Bottom) $\gamma = 10^{-2}$ (closer to the case of CO_2 lasers).

shots of the evolution of the pattern. Up to now, and to the best of our knowledge, no instantaneous two-dimensional (2D) measurements have been done in VCSELs. However, instantaneous patterns have been measured in other class-B lasers as CO_2 and Nd:YAG lasers showing a very different dynamics. Besides modelike patterns having not been observed in high Fresnel CO_2 lasers, the characteristic size of the structures present in the spatial profile does not change during the whole evolution of the system [3,4]. On the contrary, the recorded patterns for the case of the Nd:YAG laser do not show the same length scale along the pulse. The ratio between electric field decay rate κ and inversion population decay rate $\gamma_{||}$ in CO_2 lasers is around 0.1 while the ratio in Nd:YAG lasers is of the order of 10^{-5} . We think that this extreme difference of ratios is the relevant factor to explain the differences between both dynamics. To test this hypothesis we have integrated numerically the system of Eqs. (1) and (2) with values of $\gamma = \gamma_{||} / \kappa$ closer to the case of CO_2 lasers. We find that the lifetime of the ordered regime is decreasing as γ increases. Some representative instantaneous patterns, showing the evolution of the spatial intensity profile along the pulse, can be seen in Fig. 7 for values of γ of 10^{-4} and 10^{-2} . While the former case still presents modelike patterns in the beginning of the time evolution, the later value of 10^{-2} causes this ordered regime to almost disappear, being confined to the very beginning of the laser pulse. This points out that the duration of different pattern dynamics depends on the ratio between the decay rates $\gamma_{||}$ and κ , even though all

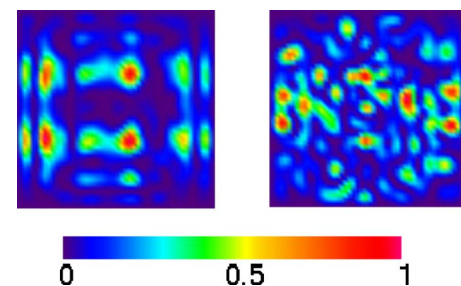


FIG. 8. (Color online) Simulated instantaneous patterns showing the transition to disorder in a broad area CO_2 laser. (a) for 40 ns and (b) for 145 ns.

cases can be classified as class-B lasers. This result could explain why an ordered phase has not been observed in the time-resolved patterns measured in CO₂ lasers [3,4]. In order to corroborate this idea we have numerically solved the laser equations used in those previous works [3,4]. We take the same parameter values used in those works and we analyze in more detail the instantaneous patterns at the beginning of the laser pulse. Effectively, we obtain that ordered patterns appear during a very short time from the beginning of the output pulse as can be seen in Fig. 8. In particular, the duration of the ordered phase is close to 70 ns. This explains why this ordered phase was not experimentally observed since the optical switching device used to measure the instantaneous patterns did not allow for the measurement of patterns at such early stages of the evolution.

VI. CONCLUSIONS

In conclusion, we have observed in a Nd:YAG class-B laser a dynamical transition from boundary-controlled patterns, consisting of high-order Gaussian-Hermite modes, to a turbulentlike regime in which bulk parameters and nonlinearities dominate the dynamics. At the first steps of the output pulse, a great variety of highly ordered spatial profiles appear, such as Gaussian-Hermite modes, stripelike modes, and flowerlike modes. At larger times, irregular patterns ap-

pear with a characteristic length scale smaller than one corresponding to the high-order modes. To the authors knowledge, this is the first time where a dynamical transition from order to turbulence is observed in class-B lasers, without the modification of the Fresnel number. Neither the stationary patterns in VCSELs nor the time-resolved measurements in CO₂ lasers have showed this dynamical transition. This transition shows that the Fresnel number and frequency separation between transverse modes are not enough to classify spatial dynamics into ordered or disordered ones. The system can show both types of dynamics along the evolution of the output pulse, being the pumping and the ratio between constant decay rates the fundamental parameters that determine the duration of each regime. This dependence explains why this transition has not been observed previously in other class-B lasers such as a CO₂ laser. Simulations within the framework of semiclassical theory reproduce the main features of the experimental results, which demonstrate the validity of the Maxwell-Bloch equations to handle the fundamental features of spatial dynamics in lasers.

ACKNOWLEDGMENTS

We wish to acknowledge P. Hoess and J. Alonso for technical support. This work was supported by Project No. BFM2003-06292 (Spain).

-
- [1] R. D. Dubois and L. H. Toburen, *Phys. Rev. A* **38**, 3960 (1988).
 - [2] Y. F. Chen and Y. P. Lan, *Phys. Rev. A* **64**, 063807 (2001).
 - [3] F. Encinas-Sanz, I. Leyva, and J. M. Guerra, *Phys. Rev. Lett.* **84**, 883 (2000).
 - [4] F. Encinas-Sanz, S. Melle, and O. G. Calderón, *Phys. Rev. Lett.* **93**, 213904 (2004).
 - [5] F. Quintero, J. Pou, F. Lusquis, M. Larosi, R. Soto, and M. Pez-Amor, *J. Laser Appl.* **12**, 84 (2001).
 - [6] R. M. Pick and M. D. Colvard, *J. Periodontol.* **64**, 589 (1993).
 - [7] M. Grabherr, R. Jäger, M. Miller, C. Thalmaier, J. Herlein, R. Michalzik, and K. J. Ebeling, *IEEE Photonics Technol. Lett.* **10**, 1061 (1998).
 - [8] S. P. Hegarty, G. Huyet, J. G. McInerney, and K. D. Choquette, *Phys. Rev. Lett.* **82**, 1434 (1999).
 - [9] T. Ackemann, S. Barland, M. Cara, S. Balle, J. R. Tredicce, R. Jäger, M. Grabherr, M. Miller, and K. J. Ebeling, *J. Opt. B: Quantum Semiclassical Opt.* **2**, 406 (2000).
 - [10] I. V. Babushkin, N. A. Loiko, and T. Ackemann, *Phys. Rev. E* **69**, 066205 (2004).
 - [11] Y. F. Chen and Y. P. Lan, *Phys. Rev. A* **65**, 013802 (2002).
 - [12] D. Dangoisse, D. Hennequin, C. Lepers, E. Louvergneaux, and P. Glorieux, *Phys. Rev. A* **46**, 5955 (1992).
 - [13] E. Louvergneaux, D. Hennequin, D. Dangoisse, and P. Glorieux, *Phys. Rev. A* **53**, 4435 (1996).
 - [14] G. Huyet, M. C. Martinoni, J. R. Tredicce, and S. Rica, *Phys. Rev. Lett.* **75**, 4027 (1995).
 - [15] G. Huyet and J. R. Tredicce, *Physica D* **96**, 209 (1996).
 - [16] I. Fischer, O. Hess, W. Elsässer, and E. Göbel, *Europhys. Lett.* **35**, 579 (1996).
 - [17] F. Hollinger, Chr. Jung, and H. Weber, *Opt. Commun.* **75**, 84 (1990).
 - [18] O. G. Calderón, V. M. Pérez-García, I. Martín, and J. M. Guerra, *Phys. Rev. A* **53**, 3490 (1996).
 - [19] G. Anstett, M. Nittmann, A. Borsutzky, and R. Wallenstein, *Appl. Phys. B: Lasers Opt.* **76**, 833 (2003).
 - [20] Y. F. Chen, K. F. Huang, H. C. Lai, and Y. P. Lan, *Phys. Rev. Lett.* **90**, 053904 (2003).
 - [21] Y. F. Chen, K. F. Huang, and Y. P. Lan, *Phys. Rev. E* **66**, 046215 (2002).
 - [22] A. E. Siegman, *Lasers* (Oxford University, London 1986).
 - [23] E. Roldán, G. J. de Valcárcel, J. F. Urchuegá, and J. M. Guerra, *J. Opt. Soc. Am. B* **20**, 816 (2003).